Ion Channel Formation by Amyloid-β_{42} Oligomers but not Amyloid-β_{40} in Cellular Membranes

David C Bode, Mark D Baker*, John H Viles*

From the School of Biological and Chemical Sciences & the Blizard Institute, Queen Mary, University of London

Running Title: Differential ion channel formation by $A\beta_{40}$ and $A\beta_{42}$

*To whom correspondence should be addressed: John H. Viles, SBCS, Queen Mary, University of London, Mile End Road, London E1 4NS, UK. Telephone: +44 (0)20 7882 8443. Email: j.viles@qmul.ac.uk and Mark. D. Baker, Blizard Institute, Centre for Neuroscience and Trauma, Barts and The London School of Medicine and Dentistry, 4 Newark Street, London, E1 2AT. Telephone: +44 (0)20 7882 2483. Email: m.d.baker@qmul.ac.uk

Keywords: Alzheimer's Disease; Aβ; Ion channels; Pores; Oligomer; Cell membrane; Toxicity

ABSTRACT:

A central hallmark of Alzheimer's disease (AD) is the presence of extracellular amyloid plaques chiefly consisting of amyloid-β (Aβ) peptides in the brain interstitium. Aβ largely exists in two isoforms, 40 or 42 amino acids long, while a large body of evidence points to Aβ(1-42) rather than Aβ(1-40) as the cytotoxic form. One proposed mechanism by which Aβ exerts toxicity is the formation of ion channel pores that disrupt intracellular Ca^{2+} homeostasis. However, previous studies using membrane mimetics have not identified any notable difference in the channel-forming properties between Aβ(1-40) and Aβ(1-42). Here, we tested whether a more physiological environment—membranes excised from HEK293 cells of neuronal origin—would reveal differences in the relative channel-forming ability of monomeric, oligomeric, and fibrillar forms of both Aβ(1-40) and Aβ(1-42). Aβ preparations were characterized with transmission electron microscopy and Thioflavin-T fluorescence. Aβ was then exposed to the extracellular face of excised membranes and transmembrane currents were monitored using patch-clamp. Our data indicated that Aβ(1-42) assemblies in oligomeric preparations form voltage-independent, non-selective ion channels. In contrast, Aβ(1-40) oligomers, fibres and monomers did not form channels. Ion channel conductance results suggested that Aβ(1-42) oligomers—but not monomers and fibres—formed 3 distinct pore structures with 1.7, 2.1, and 2.4 nm pore diameters. Our findings demonstrate that only Aβ(1-42) contains unique structural features that facilitate membrane insertion and channel formation, now aligning ion channel formation with the differential neurotoxic effect of Aβ(1-40) and Aβ(1-42) in AD.

INTRODUCTION

Alzheimer's disease (AD) is the most prevalent fatal neurodegenerative disease worldwide and accounts for up to 80% of all dementia cases. Global forecasts estimate the total number of people living with dementia to grow from 47 to 132 million by 2050 (1). Amyloid-β (Aβ) peptide is a principal component of extracellular amyloid plaques found in the brain interstitium and a key hallmark of AD. A critical step in disease progression is in the misfolding and self-assembly of monomeric Aβ(1-42) into oligomeric, and fibrillar aggregates (2).

The major Aβ alloforms found in extraneuronal plaque deposits are Aβ(1-40), and the less prevalent Aβ(1-42), which accounts for approximately 10% of secreted Aβ (3). However, a range of evidence points to Aβ(1-42) as the principal neurotoxic form of Aβ. Familial mutations which result in early-onset AD, cause an increase in the ratio of Aβ(1-42) to Aβ(1-40) (4). Elevated Aβ(1-42) plasma levels have also been correlated with the progression of late-onset forms of the disease (5). Aβ(1-42) is significantly more neurotoxic than Aβ(1-40) both *in vivo*, and also in neuronal cell culture (6-9), whilst memory impairment is believed to be driven by Aβ(1-42) disruption of long term potentiation (LTP) (10,11).

The mechanism of Aβ(1-42)-associated synaptic dysfunction remains poorly defined (8), although Aβ-associated membrane disruption has been linked to extracellular cytotoxicity by impairment of calcium homeostasis (12-14). Aβ-induced membrane disruption is suggested to occur by breaking the dielectric barrier of the membrane; through thinning and even puncturing of the membrane (15,16), or through insertion and formation of stable ion channel pore assemblies which span the cell membrane (17-19). The channel forming capability of Aβ was first described using artificial lipid bilayers. Stepwise electrical currents indicative of ion channel activity were recorded on bilayer exposure to lipid vesicle-reconstituted Aβ(1-40) (17). Further studies in artificial bilayers have supported this finding with Ca^{2+}- sensitive fluorescence and voltage-clamp current recording using both Aβ(1-40) (18-21) and Aβ(1-42) (22-27). Recently, detailed comparisons of cytotoxicity and membrane perforations have also been described for various Aβ fragments; Aβ(1-28), Aβ(25-35) and Aβ(17-42). Although in this study, channel-like open and close behaviour is not described (14).

A selection of commonly shared channel features is as follows. Aβ channels are large in size (with a conductance often greater than 250 pS), remain open for long periods of time (>500 ms), display spontaneous voltage-independent activation, and transition between multiple conductance states (28,29). There is also structural evidence to support the ion channel hypothesis. Channel-resembling structures composed of Aβ have been shown to span supported lipid bilayers by atomic force microscopy (AFM) (19,25,30), these findings are thought to be dependent on the formation of annular pore-like Aβ assemblies with an 8-25 nm outer diameter and a 2-6 nm pore opening (31,32). Similar annular oligomers have been reported for α-synuclein from Parkinson's disease, which are also capable of forming ion channels (31,33,34). A shared mechanism of ion pore toxicity has therefore been proposed (31).

Despite the reported differential synaptotoxic effect of Aβ(1-40) and Aβ(1-42), ion channel studies have largely focused on artificial lipid bilayers and little data exists to directly compare channel forming properties of different Aβ isoforms in a cellular membrane preparation. Furthermore, the majority of ion channel studies were performed before the importance of assembly state in neurotoxicity was fully appreciated. Attention has

shifted to a series of Aβ(1-42) oligomers ranging from 9 –200 kDa which are proven to be more toxic than monomeric and fibrillar forms of Aβ(1-42) (10,11,35,36). Here, we assess the relative channel forming ability and properties of a series of Aβ(1-40) and Aβ(1-42) preparations in membrane patches excised from a HEK293 immortalized cell line. For oligomeric preparations of Aβ(1-42) we recorded large, non-selective ion channels, but channels were not observed for monomeric or purified fibrillar forms of Aβ(1-42). While, neither monomeric, oligomeric or fibrillar forms of Aβ(1-40) formed ion channels under the same conditions. Our observations make a direct link between the unique ability of Aβ(1-42) assemblies to form ion channels with a known *in vivo* synaptotoxicity for Aβ(1-42), but not Aβ(1-40).

RESULTS

Aβ ion channels are observed with oligomeric Aβ(1-42) but not oligomeric Aβ(1-40) - Patch-pipettes were backfilled with 5 μM Aβ preparations. Patches of membrane were then excised from HEK293 cells and Aβ was free to diffuse towards the extracellular face of the membrane within the pipette. Transmembrane currents were measured by clamping the patch at a series of step-voltage potentials. Six different Aβ preparations were studied, with between 20 and 49 patches of membrane pulled for each. Monomer, oligomer and fibre preparations of both Aβ(1-40) and Aβ(1-42) were studied. The assembly state of Aβ is critical in exerting synaptic dysfunction and neurotoxicity, it was therefore important to carefully characterise the Aβ assembly types that were presented to membrane patches. Aβ preparations have been characterised using transmission electron microscopy (TEM), size-exclusion chromatography (SEC) and the fibre specific Thioflavin T (ThT) fluorescent dye (Fig. 1).

Large, voltage-independent Aβ channels with clear open/close step-current transitions form in the presence of oligomeric and fibrillar Aβ(1-42) assemblies (Fig. 1e,f). Channels were found in 17 of 49 (35%) patches with Aβ(1-42) oligomer and 8 of 24 patches (33%) with Aβ(1-42) fibre when monitored for 30 minutes. Importantly, ion channels were not observed for SEC purified Aβ(1-42) monomer (n=24) (Fig. 1d). We next wanted to determine whether channels formed by Aβ(1-42) fibre preparations were in fact due to the presence of small oligomers observed to co-exist in Aβ(1-42) fibre preparations by TEM (Fig. 1f). Oligomers were removed from the fibre preparation by centrifugation. The pelleted Aβ(1-42) fibres were then re-suspended into patch clamp buffer for delivery to the membrane at 5 μM. The channel forming ability of the oligomer-depleted Aβ(1-42) fibres was significantly reduced, relative to the un-purified fibre sample, with only one channel observed in 24 patches (4%).

We also exposed the excised membranes to Aβ(1-40) and found that Aβ(1-40) monomer (n = 20), oligomer (n = 20) and fibre (n = 20) preparations did not form any Aβ-associated ion channels, also in a 30 minute recording period. Aβ channels were also not present in Aβ-free buffer exposed control patches (n = 20). Fisher's exact tests including Bonferroni correction showed channel formation by Aβ(1-42) oligomers to be significant against Aβ(1-40) oligomer ($p = 0.002$) and Aβ(1-42) monomer ($p = 0.0007$). Also, Aβ(1-42) fibre preparations were significantly different in their ability to form channels from Aβ(1-40) fibres ($p = 0.005$). However, removal of oligomers from Aβ(1-42) fibre samples reduced the probability of ion channel formation significantly, when compared to un-centrifuged Aβ(1-42) fibres preparations which contained oligomers ($p = 0.01$) (Fig. 2).

Next, we wanted to investigate the ion channel forming properties of a more dilute Aβ(1-42) oligomer preparation. A ten-fold dilution at 0.5 μM monomer equivalent concentration of Aβ(1-42) oligomers was delivered to membranes and channel currents were observed in as many as 6 of 40 patches (15%). A further ten-fold dilution to 50 nM caused some reduction in the number of channels observed, but not proportional to the one-hundred-fold dilution factor with channels observed in 10% of patches (n = 20).

Endogenous ion channels were observed for many, but not all, membrane patches; they were much smaller in size, typically less than 85 pS, and exhibited voltage-dependent activation (Fig. 3). Aβ channels were markedly larger in size, with the smallest observed channel exhibiting a conductance of 270 pS.

Aβ(1-42) channel conductance, pore diameter and rate of formation - Channels formed by Aβ(1-42) oligomer commonly remained stable in the membrane for a period of many minutes (≥10 minutes), open times were frequently in excess of 1.5 seconds, a value limited only by the duration of the applied voltage-clamp protocol. The majority of channels exhibited flicker in which the channel transitioned briefly to lower conductance levels, Fig. 4a. Flicker transitions are observer at all applied depolarizing and hyperpolarizing potentials.

Typical current traces recorded for Aβ(1-42) oligomers are shown in Fig. 5a, for three representative channels that exhibit three distinct conductances. Open/close step current transitions at each clamped membrane potential were measured to determine operating channel conductance by generating a current/voltage relationship (37). The straight-line fits used to determine the mean conductance of each channel are shown in Fig. 5b.

A plot showing the distribution of channel conductance, Fig. 5c, for a total of 34 different channels indicates Aβ(1-42) oligomers form three or more distinct channel sizes. The primary channel-type (35% of channels) produced a median conductance of 337 pS (ranging between 310 - 350 pS), with at least two more subgroups of channels exhibiting 490 pS (477- 497 pS) and 627 pS (608 - 642 pS) conductance. In some cases, channel currents transition between two primary channel sizes, Fig 4b. Current measurements were therefore made from the most commonly observed state in which the channel remains stable.

Approximate pore size can be calculated from the channel conductance, assuming the pore is cylindrical with a bilayer spanning length assumed to be 7 nm (38). This model has been adapted to estimate channel diameter in large ion channels, see experimental procedures, Eq.1. Using Eq.1, the three channel subtypes have an estimated pore diameter of 1.7 nm, 2.1 nm and 2.4 nm respectively, Fig. 5c. Groupings of conductance indicate discrete channel sizes with narrow ranges of diameters: 1.62-1.73 nm; 2.04-2.09 nm; 2.34-2.41 nm. Standard deviations are 0.03 nm for all three channel types identified. There are also a limited number of channels with even higher conductance, ranging between 737 - 1039 pS with calculated diameters, between 2.6 - 3.2 nm.

On delivery of Aβ(1-42) oligomer to the membrane, channels do not form instantly, with a delay of more than 2 minutes before channel-current is observed, Fig. 6. Short-lived current spikes associated with membrane de-stabilisation would often precede the appearance of an Aβ ion channel. The bulk of the channels formed between 4 - 8 minutes following membrane exposure, with 50% of channels formed within 8.5 minutes of exposure. The rate at which channel formation occurs appears to be unrelated to channel

conductance. A Pearson correlation r value of 0.04 suggests no correlation between conductance and time elapsed before channel formation.

Channels formed with Aβ(1-42) oligomers and oligomers from un-purified fibre samples had similar electrophysiological characteristics. In particular, channels formed by Aβ(1-42) oligomer and fibre preparations were similar in size with comparable median conductances. Channels in each group formed at similar rates, with the majority arising within the first 10 minutes.

Aβ(1-42) channels are not cation selective - The Goldman-Hodgkin-Katz (GHK) equation, adapted by Spangler (39), links the concentration and permeability of Na^+, Ca^{2+}, K^+ and Cl^- ions, to the reversal potential (E_{rev}) of a membrane (37). An E_{rev} of 0 mV was measured in patches containing Aβ(1-42) ion channels in a symmetrical pipette and bath solution. The composition of ionic solution on the internal membrane face was then altered by perfusion with two separate patch clamp buffers, which had 50% (n = 2, 642 pS and 844 pS), and 75% (n = 2, 627 pS and 1039 pS) of NaCl replaced with tetraethylammonium chloride (TEACl). According to the GHK equation (see experimental procedures, Eq.2), the E_{rev} of a purely cation-selective channel would be expected to shift to +20 mV and +28 mV for each respective solution. A modest shift of +6 mV observed in each case suggests Aβ(1-42) channels permeate both anions and cations (Fig. 7a).

Evidence of non-selectivity is further supported by depletion of both anions and cations. Three more channel incorporated patches were perfused with patch clamp solution which had an 80% volume replacement with equi-molar sucrose. Under these conditions, the E_{rev} of a purely cation-selective channel would be expected to shift +40 mV (Eq.2). However, a small E_{rev} of -8 mV was measured (336, 622 and 642 pS), Fig. 7b.

DISCUSSION

The ability of Aβ to form membrane-spanning ion channels is a mechanism by which Aβ might exert synaptic neurotoxicity (17-19). However, the relationship between Aβ pore formation and AD pathology has been questioned, as previous studies have made little distinction between Aβ(1-40) and Aβ(1-42) ability to form ion channels (20,25,26,40). Hence, a mismatch has existed between observed ion channel formation by Aβ(1-40) (17-21) and what is known about the relative pathogenicity of Aβ(1-40) and Aβ(1-42) *in vivo*.

Here, we show only Aβ(1-42) oligomer preparations form channels while Aβ(1-40) oligomer and fibres do not form channels in HEK293 cell-excised membrane. Therefore, our study aligns the ion channel hypothesis of Aβ toxicity with studies which have established oligomeric Aβ(1-42) as the toxic entity of AD pathology (10,11,36,41). Furthermore, we provide evidence to suggest monomeric Aβ(1-42) is incapable of forming ion channels from solution whilst Aβ(1-42) oligomer will readily insert into the lipid bilayer to form membrane spanning pores.

The ion channel properties observed in this investigation are consistent with those observed in other voltage-clamp studies. In particular, they were large in size (270-1039 pS), voltage-independent and transiently flickered between multiple conductance states (17,20,29). A question remains as to why others have reported Aβ(1-40) channels (17-21,40) but we have only observed channels for Aβ(1-42). Most of the disparities in the literature may be explained by the method in which Aβ is delivered to the membrane. Aβ(1-40) channels were typically generated using peptide already reconstituted into vesicular lipid bilayers (17-19,21), and as such, channel formation would not be dependent on the insertion of Aβ into a preformed lipid bilayer. Our

data suggests the additional Al_{41}-Val_{42} residues found in Aβ(1-42) are important in the formation of cell membrane spanning ion channels. Although, there are some reports of channel formation from solution for Aβ(1-40) (20,26,40,42), the majority of these studies report Aβ insertion into artificial model bilayers rather than cellular membrane. Importantly, this is the first study to report Aβ(1-42) ion channels in excised cellular membrane and in this case membrane composition may favour Aβ(1-42) insertion given that single-molecule imaging has previously demonstrated Aβ(1-42) oligomers to have a greater affinity for hippocampal membrane than Aβ(1-40) (43). Molecular dynamics simulations also suggest Aβ(1-42) to be twice as efficient at inserting into lipid bilayers when compared to Aβ(1-40) (44). It is therefore plausible that a differential membrane interaction and insertion of Aβ isoforms may explain a lack of ion channels formed by the Aβ(1-40) preparations studied here.

Size-exclusion chromatography purified Aβ(1-42) monomer preparations did not form ion channels. Similarly, removal of low molecular weight, diffusible oligomer from Aβ(1-42) fibres almost completely removed the ability of fibre preparations to produce ion channels. This indicates channel formation to be dependent on the self-assembly of Aβ(1-42) into oligomeric structures which are capable of inserting into the membrane to form membrane spanning pores. Previous studies have assumed monomeric conformations of Aβ forming ion channels (17,18,21,24,29,40). However, monomeric Aβ preparations were not SEC-purified or structurally characterised, and the solubilisation protocols used are likely to have generated oligomeric assemblies. A more recent study has implicated a select population of 4-mer to 13-mer assemblies in triggering Aβ-induced ion flux for both Aβ(1-40) and Aβ(1-42) in planar lipid bilayers (42), however perforations were sporadic in nature. Current transitions were not well defined and open pore lifetimes as low as several milliseconds were recorded, suggesting greater pore instability compared to ion channels observed here.

Electrophysiological characterisation of Aβ channels recorded in this study allows comparisons to be made with proposed structural features of Aβ pores based on AFM micrographs. Pore size diameter can readily be estimated using a measured channel conductance.. Here, the median conductance of the three main channel subtypes were measured to be 337 pS, 490 pS and 627 pS which implies an approximate pore diameter of 1.7 nm, 2.1 nm and 2.4 nm, assuming a lipid bilayer of 7 nm. These values are closely in line with pore diameters taken from molecular dynamics simulations and AFM studies (19,25,30,45). Space-filling simulations, predict a preferred Aβ 16-mer to 24-mer channel configuration, with estimated pore diameters of ~1.6 nm and ~2.5 nm respectively (45). Recently a combination of biophysical studies (CD, protease-K digestion and solution NMR) on pore forming Aβ(1-42) oligomers has revealed data consistent with a β-barrel conformation. In the future, these preparations in a membrane mimicking environment may be amenable to 3D structure determination (27). Channels were also of comparable size to those observed by AFM, channel-resembling structures which spanned artificial lipid bilayers had 1-2 nm measured pore diameters (19,25,30). Pore-like structures of comparable scale to the larger channels formed in this study have also been observed (31,32). Annular assemblies with a 2.5- 4 nm pore diameter have been found localised to the membrane of AD model mice and human AD frontal cortex (46). Transitions between conductance states (Fig. 4b) suggest Aβ ion channels are dynamic structures which can change in pore dimensions. Similar transitions have also been reported for pores formed by the misfolding amyloid protein, α-synuclein from Parkinson's disease (33,34).

Ion channel formation follows a biphasic process; channels were not observed within the first few minutes after exposure to Aβ, this delay may represent the time taken for Aβ oligomers to insert into the membrane and perhaps undergo structural rearrangement of Aβ into membrane spanning pores. Most channels form within 10 minutes of exposure to Aβ. The mechanism by which Aβ coalesces into a membrane-spanning channel assembly is yet to be defined (22,47). Aβ is capable of forming channel resembling structures in the form of annular pore assemblies (31,32). However, pre-formed annular assemblies are surprisingly ineffective at permeabilising lipid bilayers. Instead, spherical oligomers which precede annular pores are required (32). The lack of ion channels for monomeric Aβ(1-42) may be explained by a relative inability of monomer to insert into the membrane. Indeed, previous data suggests Aβ(1-42) oligomers to preferentially interact with hippocampal cell membranes relative to Aβ(1-42) monomer (43). Neutron diffraction studies support this, as Aβ(1-42) monomer was seen not to insert into cholesterol containing bilayers, Aβ(1-42) insertion was seen only after monomeric self-assembly into oligomers (48).

Cation-selectivity has been reported for Aβ(1-40) pores (17,20,26,40). Aβ(1-42) channels formed in this study exhibited a lack of selectivity for cation, this is in agreement with a previous model lipid bilayer study (26). A difference in ion-selectivity between Aβ(1-40) and Aβ(1-42) could be due to changes in localised membrane composition. In particular, increased lipid bilayer cholesterol has been suggested to shift Aβ(1-42) channel selectivity in favour of anion permeation (49). Given that molecular dynamics simulations predict Aβ(1-42) to insert more readily into cholesterol-containing phosphatidylcholine membranes (44), the more hydrophobic Aβ(1-42) could conceivably target non-polar cholesterol raft environments and exhibit non-selectivity of ions as a result. Alternatively, cation-selectivity could be altered by changes to the structural configuration of negatively charged residues, postulated to reside in the pore lining (50,51).

A similar incidence of channel formation was observed, with channels forming in 35% and 33% of patches for Aβ(1-42) oligomer and Aβ(1-42) fibre preparations which had not had the oligomeric component depleted by centrifugation. Aβ(1-42) oligomer and fibre preparations appear to be equally effective in loading a membrane with Aβ. This is somewhat surprising, given that the concentration of free Aβ(1-42) oligomer is significantly lower in fibre preparations. This suggests the membrane is still saturated with channel forming assemblies, even at lower concentrations. This hypothesis is supported by subsequent experiments in which ten-fold diluted 500 nM Aβ(1-42) oligomer preparation also yielded channels in 15% of patches. Even when Aβ(1-42) oligomers are diluted one hundred-fold to 50 nM, an appreciable proportion of channels (10%) are observed. Therefore, at 500 nM – 5 μM, the proportions of patches in which Aβ channels formed are, to a large extent, independent of Aβ oligomer concentration.

It is interesting to speculate why, if the membrane is saturated, we only observed channels in 35% of patches. One possibility is that channel formation is dependent on bilayer composition found only within a third of patches pulled. Perhaps membrane proteins can modulate channel formation (52). Others have highlighted the importance of membrane composition for effective Aβ insertion and perforation of model lipid membranes, specifically pointing to GM1 and cholesterol as key mediators of membrane interaction and perforation (16,53,54). Such sites may be critical in the formation of ion channels in cells. Although we note ion channels formed in synthetic bilayers do not require GM1 or cholesterol (17,26).

An apparent membrane saturation would be consistent with a study which suggests that Aβ saturates a model lipid bilayer at very low peptide to lipid ratios; as little as 2 nM was enough to saturate all membrane binding sites (55). Membrane patches excised in this study have an approximate surface area of 7 μm^2. A typical neuron with a membrane surface area of 250,000 μm^2 might theoretically incorporate more than 10,000 Aβ(1-42) channels with the cytotoxic potential to increase intracellular calcium levels.

The channel forming capacity of oligomeric Aβ(1-42) assemblies, but not monomeric Aβ(1-42) or any form of Aβ(1-40), makes a direct correlation between pore formation and the known pathology of various Aβ assemblies in AD. This adds weight to the amyloid pore hypothesis and as such, molecules that block these ion channels may be therapeutic in protecting neurons against the synaptotoxic effects of Aβ.

EXPERIMENTAL PROCEDURES

Aβ Peptide Preparations and Characterisation - *Monomer:* Lyophilised Aβ(1-40) and Aβ(1-42) was purchased from Cambridge Research Biochemicals, and EZBiolab inc. Aβ peptides were synthesised using solid phase F-moc (N-(9-fluorenyl)methoxycarbonyl) chemistry, producing a single elution band in HPLC with correct mass verified by mass spectrometry. Peptides were solubilised in ultra-high quality (UHQ) water (0.7 mg/ml at pH 10.5) and left at 4 ºC for 12 hours. It was necessary, particularly in the case of Aβ(1-42), to remove any remaining nucleating, oligomeric aggregates by SEC (Superdex 75 10/300 GL column) in order to generate a seed-free preparation.

Seed-free Aβ, termed here as monomeric, had no ThT fluorescence signal and exhibited a clear lag-phase to the nucleation polymerisation reaction (Fig. 1a). Furthermore, SEC-purified Aβ gave a single elution band and assemblies were not observed by negative-stain TEM (Fig. 1). Concentration were determined by absorbance of stock solutions at 280 nm ($\varepsilon = 1280\ M^{-1}.cm^{-1}$) using a Hitachi U-3010 spectrophotometer. Monomeric samples were stored immediately after SEC elution at -80 ºC.

Fibres: Amyloid fibre preparations of Aβ(1-40) and Aβ(1-42) were generated in a 96-well plate incubation of the peptides at 10 μM, 160 mM NaCl and 30 mM HEPEs at pH 7.4. Assembly kinetics were monitored with Thioflavin T fluorescence (ThT), adjacent sample-wells with no ThT added were used in all patch clamp experiments. At equilibrium, Aβ assemblies have the typical amyloid fibrous appearance according to TEM. Aβ(1-40) fibres were many microns in length and 10-20 nm in diameter (Fig. **1c**). Aβ(1-42) is typically more heterogeneous in appearance, with oligomeric and protofibrillar assemblies present in addition to amyloid fibres (Fig **1f**).

Oligomers: Similarly, Aβ(1-40) and Aβ(1-42) assemblies with predominantly circular oligomeric structure were obtained from the well plate towards the end of the lag-phase, as monitored by ThT fluorescent dye in separate wells (Fig. 1a). Samples were immediately stored at -80 ºC to prevent further assembly. TEM images show a large number of circular oligomeric assemblies between 5 and 20 nm in diameter (Fig. **1b** and **1e**). A preparation of Aβ(1-42) oligomers and proto-fibres were also obtained for Aβ(1-42) by solubilising at pH 10.5, but these samples were not purified by SEC. These oligomer samples did not have a clear lag-phase before elongation of fibres (Fig. 1a). Numerous protofibrillar assemblies were also present, typically 200 nm long, in addition to a limited number of short fibres.

Oligomer-depleted fibres: Oligomer-depleted fibre preparations were generated by centrifugation of Aβ(1-42) fibre samples at

16,100 g for 5 minutes as previously described (56). The supernatant which contained small diffusible oligomers was removed, and the fibre pellet re-suspended for use in additional patch clamp experiments at a final concentration of 5 µM.

Aβ Assembly - ThT fluorescence upon fibre formation was measured using BMG-Galaxy and BMG-Omega FLUOstar fluorescence 96-well plate readers. Well plates were subjected to mild double orbital shaking for 30 seconds every 30 minutes followed by a fluorescence reading, 20 flashes per well, per cycle with 4 mm orbital averaging. Fluorescence excitation and emission detection were at 440 nm and 490 nm respectively. ThT fluoresces when bound to amyloid fibres to give a fluorescent signal proportional to the amount of amyloid fibre present. It has been shown that ThT does not markedly effect the formation or kinetics of fibres (57).

Size-exclusion chromatography (SEC) - A superdex 75 10/300 GL column (GE Healthcare) was used to purify and elute a monomeric fraction of solubilised Aβ preparations using AKTA FPLC. A stock 90 µM Aβ solution in UHQ water was loaded onto the column and the monomer peak was eluted in a solution of 160 mM NaCl, 30 mM HEPES using a 0.5 ml/min flow rate at 4 ºC. Eluted monomer had a typical concentration of 30 µM.

Transmission electron microscopy (TEM) - Aβ containing preparations were aliquoted (5 µl) onto glow-discharged carbon-coated 300-mesh grids using the droplet method, washed with UHQ water, then a negative phosphotungstic acid (2% w/v, pH 7.4) stain was applied before a final wash step. Images were taken with a JEOL JEM-1230 electron microscope operated at 80 keV paired with the Olympus iTEM software package. Representative images were selected from multiple images taken across multiple grids and fields.

Cell culture - HEK293 immortal cells of neuronal origin were cultured in 30 ml cell culture flasks. Cells were grown in a 37 ºC, 5% CO_2 incubator in Dulbecco's Modified Eagle Medium (DMEM) supplemented with 10% fetal bovine serum and penicillin-streptomycin (200 units and 0.2 mg/ml respectively). On reaching confluence, Ca^{2+} and Mg^{2+}-free phosphate-buffered saline (pH 7.2) was used to dissociate cells from culture flasks for splitting. Cultured cells were split every 5-7 days and used between passage 22 to 65. With each round of splitting, a fraction of cells was plated into 35-mm diameter Petri dishes and maintained in supplemented DMEM until the day of a patch clamp experiment. Plated cells were cultured for 2-3 days before use in patch clamp experiments. Reagents and media were purchased from Sigma-Aldrich and ThermoFisher scientific (Invitrogen).

Patch clamp recording - Patch clamp recordings in voltage-clamp mode were made from excised membrane of HEK293 cells. Patch pipettes were backfilled with patch clamp buffer containing a series of Aβ preparations containing 5 µM, 500 nM or 50 nM, monomer equivalent concentration of Aβ at pH 7.4. Aβ was free to diffuse towards the extracellular face of the membrane within the patch pipette and transmembrane currents were measured by clamping the patch at a series of voltage-potentials between +60 and -60 mV. Patches of membrane were excised, in an inside-out configuration, into a 35 mm dish containing buffer of identical ionic composition.

A stepwise voltage-ramp protocol using an Axopatch 200B amplifier (Axon Instruments, Union City, CA, USA) was applied via PC using PCLAMP-10 software (Axon Instruments). Data was further processed using a Clampfit software package, and a lowpass boxcar filter was typically applied. Patches were pulled from thick-walled filament borosilicate glass (Harvard Apparatus, Edenbridge, Kent, UK) with a needle diameter of approximately 1–3 µm and a resistance of 4-6 MΩ

when filled with recording solution. Junction potentials generated at boundaries of ionic asymmetry were accounted for using an applied pipette offset potential. Recordings were sampled at a rate of 2 kHz with 500 µs intervals with a lowpass 4-pole Bessel filter frequency of 1 kHz.

In excised-patch, the holding potential was set to 0 mV. Recordings were made in symmetrical solution adjusted to pH 7.4, containing (mM): 121.4 NaCl, 10 CsCl, 9 NaHEPEs, 1.85 $CaCl_2$, 1.87 $MgCl_2$, 2.16 KCl, and 0.1 EGTA. Transmembrane patch currents were recorded for 30 minutes, if current spikes indicative of membrane de-stabilisation were observed in this time period, the recordings were extended to 45 minutes. The majority, 90 % of channels, were formed within the first 30 mins.

Channel current transitions between open/closed states were measured using Clampfit software at each membrane potential. An average from typically 5 measurements for any given membrane potential was made to generate a current voltage (I/V) relationship. The slope of the I/V relationship was calculated to estimate channel conductance (pS). Each conductance value for an individual channel is obtained from typically five or more current measurement values at the six different potentials; a straight line is then fitted to the >30 data points to obtain the conductance value. Fisher's exact tests (SPSS software) were performed with a Bonferroni correction to assess statistical significance comparing each Aβ preparation (58).

Calculation of channel pore diameter using channel conductance - Theoretical pore diameter has been calculated using a model developed by Hille (38) and adapted by Cruickshank et al (59). Pore diameter (d) is calculated in a solution of defined resistivity (ρ), for a pore of measured length (l) and ionic conductance (g) (Equation. 1). A membrane-spanning conformation with a pore length (l) of 7 nm (45,51) and a solution resistivity of 80 Ω cm has been assumed (60).

$$\boldsymbol{d = \frac{\rho g}{\pi}\left(\frac{\pi}{2} + \sqrt{\frac{\pi^2}{4} + \frac{4\pi l}{\rho g}}\right)}$$

(Eq . 1)

Calculation of channel selectivity - Patches were pulled in solution of symmetrical ionic composition, and then ionic concentration gradients were generated by gravity perfusion of solutions of altered composition on to the internal face of the membrane. Ion channel selectivity was probed by measurement of a reversal potential.

Channel selectivity has been calculated using a modified Goldman-Hodgkin-Katz equation (39) (eq.2). The Goldman-Hodgkin Katz equation (Eq.2) has been used to predict membrane reversal potential (E_{rev}) given the concentration and permeability (P) of ions on the intracellular ($[ion]_{int}$) and extracellular ($[ion]_{ext}$) face of a membrane. The reversal potential is the membrane potential in which ions are at equilibrium and zero current flows. E_{rev} measured in the current investigation deviated from an expected E_{rev} according to previous studies. The cation-selective ion-permeability ratio of Na^+:1; K^+:1.3; Ca^{2+}: 1.3; Cs^+: 2 calculated by Arispe and colleagues (17) was used to predict an expected E_{rev} under our own experimental conditions

Junction potentials appearing on ion replacement were nulled by zeroing the holding current at 0 mV, and assumed no ionic selectivity for the patch leakage current. Measured channel currents are normalized against their maximum recorded channel current.

$$\boldsymbol{E_{rev} = (-RT/F)\, x\, (2.303)\, log\, 10y}$$

(Eq . 2)

R= universal gas constant, 8.314 $J.K^{-1}.mol^{-}1$; T= temperature, 296 K; F= Faraday constant, 96485$C.mol^{-1}$. Where:

$$y = \frac{-b+\sqrt{b^2-4ac}}{2a}$$

and:

$$a = 4P_{Ca}[Ca]_{ext} + 4P_{Mg}[Mg]_{ext} + P_{Na}[Na]_{ext} + P_K[K]_{ext} + P_{Cs}[Cs]_{ext} - P_{Cl}[Cl]_{int}$$

$$b = (P_{Na}[Na]_{ext} + P_K[K]_{ext} + P_{Cs}[Cs]_{ext}) - (P_{Na}[Na]_{int} + P_K[K]_{int} + P_{Cs}[Cs]_{int}) + (P_{Cl}[Cl]_{int} - P_{Cl}[Cl]_{ext})$$

$$c = -(4P_{Ca}[Ca]_{int} + 4P_{Mg}[Mg]_{int} + P_{Na}[Na]_{int} + P_K[K]_{int} + P_{Cs}[Cs]_{int} - P_{Cl}[Cl]_{ext})$$

Acknowledgements:

We thank Nadine Younan and Joseph Barritt for their expertise and technical assistance in TEM and SEC.

Conflict of interest: The authors declare that they have no conflicts of interest with the contents of this article.

Author contributions: DCB designed and conducted all experiments, analysed results and co-wrote the paper. MDB and JHV designed and analysed experiments and co-wrote the paper.

References

1. Prince, M., Wimo, A., Guerchet, M., Gemma-Claire, A., Wu, Y.-T., and Prina, M. (2015) World Alzheimer Report 2015: The Global Impact of Dementia - An analysis of prevalence, incidence, cost and trends. *Alzheimer's Disease International*, 84
2. Hardy, J. A., and Higgins, G. A. (1992) Alzheimer's disease: the amyloid cascade hypothesis. *Science* **256**, 184-185
3. Gravina, S. A., Libin, H., B, E. C., E, L. K., Laszlo, O., H, Y. L., Nobuhiro, S., and G, Y. S. (1995) Amyloid-β protein (Aβ) in Alzheimer's disease brain: Biochemical and immunocytochemical analysis with antibodies specific for forms ending at Aβ40 or Aβ42(43). *Journal of Biological Chemistry* **270**, 7013--7016
4. Suzuki, N., Cheung, T. T., Cai, X. D., Odaka, A., Otvos, L., Eckman, C., Golde, T. E., and Younkin, S. G. (1994) An increased percentage of long amyloid beta protein secreted by familial amyloid beta protein precursor (beta APP717) mutants. *Science (New York, N.Y.)* **264**, 1336--1340
5. Mayeux, R., Tang, M. X., Jacobs, D. M., Manly, J., Bell, K., Merchant, C., Small, S. A., Stern, Y., Wisniewski, H. M., and Mehta, P. D. (1999) Plasma amyloid beta-peptide 1-42 and incipient Alzheimer's disease. *Ann Neurol* **46**, 412-416
6. Dahlgren, K. N., and Manelli, A. M. (2002) Oligomeric and fibrillar species of amyloid-beta peptides differentially affect neuronal viability. *Journal of Biological Chemistry* **277**, 32046--32053

7. Klein, A. M., Kowall, N. W., and Ferrante, R. J. (1999) Neurotoxicity and oxidative damage of beta amyloid 1-42 versus beta amyloid 1-40 in the mouse cerebral cortex. *Ann N Y Acad Sci* **893**, 314-320
8. Benilova, I., Karran, E., and De Strooper, B. (2012) The toxic Aβ oligomer and Alzheimer's disease: an emperor in need of clothes. *Nat Neurosci* **15**, 349-357
9. Kuperstein, I., Broersen, K., Benilova, I., Rozenski, J., Jonckheere, W., Debulpaep, M., Vandersteen, A., Segers-Nolten, I., Van Der Werf, K., Subramaniam, V., Braeken, D., Callewaert, G., Bartic, C., D'Hooge, R., Martins, I. C., Rousseau, F., Schymkowitz, J., and De Strooper, B. (2010) Neurotoxicity of Alzheimer's disease Aβ peptides is induced by small changes in the Aβ42 to Aβ40 ratio. *EMBO J* **29**, 3408-3420
10. Lambert, M. P., Barlow, A. K., Chromy, B. A., Edwards, C., Freed, R., Liosatos, M., Morgan, T. E., Rozovsky, I., Trommer, B., Viola, K. L., Wals, P., Zhang, C., Finch, C. E., Krafft, G. A., and Klein, W. L. (1998) Diffusible, nonfibrillar ligands derived from Abeta1-42 are potent central nervous system neurotoxins. *Proceedings of the National Academy of Sciences of the United States of America* **95**, 6448--6453
11. Walsh, D. M., Klyubin, I., Fadeeva, J. V., Cullen, W. K., Anwyl, R., Wolfe, M. S., Rowan, M. J., and Selkoe, D. J. (2002) Naturally secreted oligomers of amyloid beta protein potently inhibit hippocampal long-term potentiation in vivo. *Nature* **416**, 535-539
12. Demuro, A., Mina, E., Kayed, R., Milton, S. C., Parker, I., and Glabe, C. G. (2005) Calcium dysregulation and membrane disruption as a ubiquitous neurotoxic mechanism of soluble amyloid oligomers. *J Biol Chem* **280**, 17294-17300
13. Bezprozvanny, I., and Mattson, M. P. (2008) Neuronal calcium mishandling and the pathogenesis of Alzheimer's disease. *Trends Neurosci* **31**, 454-463
14. Peters, C., Bascuñán, D., Opazo, C., and Aguayo, L. G. (2016) Differential Membrane Toxicity of Amyloid-β Fragments by Pore Forming Mechanisms. *J Alzheimers Dis* **51**, 689-699
15. Kayed, R., Sokolov, Y., Edmonds, B., McIntire, T. M., Milton, S. C., Hall, J. E., and Glabe, C. G. (2004) Permeabilization of lipid bilayers is a common conformation-dependent activity of soluble amyloid oligomers in protein misfolding diseases. *J Biol Chem* **279**, 46363-46366
16. Williams, T. L., and Serpell, L. C. (2011) Membrane and surface interactions of Alzheimer's Aβ peptide--insights into the mechanism of cytotoxicity. *FEBS J* **278**, 3905-3917
17. Arispe, N., Rojas, E., and Pollard, H. B. (1993) Alzheimer disease amyloid beta protein forms calcium channels in bilayer membranes: blockade by tromethamine and aluminum. *Proceedings of the National Academy of Sciences of the United States of America* **90**, 567--571
18. Arispe, N., Pollard, H. B., and Rojas, E. (1996) Zn2+ interaction with Alzheimer amyloid beta protein calcium channels. *Proceedings of the National Academy of Sciences of the United States of America* **93**, 1710--1715
19. Quist, A., Doudevski, I., Lin, H., Azimova, R., NG, D., Frangione, B., Kagan, B., Ghiso, J., and Lal, R. (2005) Amyloid ion channels: a common structural link for protein-misfolding disease. *Proceedings of the National Academy of Sciences of the United States of America* **102**, 10427--10432
20. Kourie, J. I., Henry, C. L., and Farrelly, P. (2001) Diversity of amyloid-beta protein fragment 1-40 -formed channels. *Cellular and Molecular Neurobiology* **21**, 255--284
21. Lin, H., J, Z. Y., and Lal, R. (1999) Amyloid-β protein (1-40) forms calcium-permeable, Zn2+-sensitive channel in reconstituted lipid vesicles. *Biochemistry* **38**, 11189--11196
22. Capone, R., Jang, H., Kotler, S. A., Kagan, B. L., Nussinov, R., and Lal, R. (2012) Probing structural features of Alzheimers amyloid-β pores in bilayers using site-specific amino acid substitutions. *Biochemistry* **51**, 776--785

23. Rhee, S. K., Quist, A. P., and Lal, R. (1998) Amyloid-β protein-(1-42) forms calcium-permeable, Zn2+-sensitive channel. *Journal of Biological Chemistry* **273**, 13379--13382
24. Bahadi, R., Farrelly, P. V., Kenna, B. L., Curtain, C. C., Masters, C. L., Cappai, R., Barnham, K. J., and Kourie, J. I. (2003) Cu2+-induced modification of the kinetics of A beta(1-42) channels. *American journal of physiology. Cell physiology* **285**, C873--C880
25. Lin, H., Bhatia, R., and Lal, R. (2001) Amyloid-beta protein forms ion channels: implications for Alzheimer's disease pathophysiology. *The FASEB Journal* **15**, 2433--2444
26. Hirakura, Y., Lin, M. C., and Kagan, B. L. (1999) Alzheimer amyloid-beta 1-42 channels: effects of solvent, pH, and Congo Red. *Journal of neuroscience research* **57**, 458--466
27. Serra-Batiste, M., Ninot-Pedrosa, M., Bayoumi, M., Gairí, M., Maglia, G., and Carulla, N. (2016) Aβ42 assembles into specific β-barrel pore-forming

oligomers in membrane-mimicking environments.
28. Kourie, J. I., Culverson, A. L., Farrelly, P. V., Henry, C. L., and Laohachai, K. N. (2002) Heterogeneous amyloid-formed ion channels as a common cytotoxic mechanism: implications for therapeutic strategies against amyloidosis. *Cell biochemistry and biophysics* **36**, 191--207
29. Arispe, N., Diaz, J. C., and Simakova, O. (2007) Abeta ion channels. Prospects for treating Alzheimer's disease with Abeta channel blockers. *Biochim Biophys Acta* **1768**, 1952-1965
30. Jang, H., Arce, F. T., Ramachandran, S., Capone, R., Azimova, R., Kagan, B. L., Nussinov, R., and Lal, R. (2010) Truncated beta-amyloid peptide channels provide an alternative mechanism for Alzheimer's Disease and Down syndrome. *Proceedings of the National Academy of Sciences of the United States of America* **107**, 6538--6543
31. Lashuel, H. A., Hartley, D., Petre, B. M., Walz, T., and Lansbury, P. T. (2002) Neurodegenerative disease: Amyloid pores from pathogenic mutations. *Nature* **418**, 291--291
32. Kayed, R., Pensalfini, A., Margol, L., Sokolov, Y., Sarsoza, F., Head, E., Hall, J., and Glabe, C. (2009) Annular protofibrils area structurally and functionally distinct type of amyloid oligomer. *Journal of Biological Chemistry* **284**, 4230--4237
33. Tosatto, L., Andrighetti, A. O., Plotegher, N., Antonini, V., Tessari, I., Ricci, L., Bubacco, L., and Dalla Serra, M. (2012) Alpha-synuclein pore forming activity upon membrane association. *Biochim Biophys Acta* **1818**, 2876-2883
34. Kim, H. Y., Cho, M. K., Kumar, A., Maier, E., Siebenhaar, C., Becker, S., Fernandez, C. O., Lashuel, H. A., Benz, R., Lange, A., and Zweckstetter, M. (2009) Structural properties of pore-forming oligomers of alpha-synuclein. *J Am Chem Soc* **131**, 17482-17489
35. Haass, C., and Selkoe, D. J. (2007) Soluble protein oligomers in neurodegeneration: lessons from the Alzheimer's amyloid beta-peptide. *Nature reviews. Molecular cell biology* **8**, 101--112
36. Brouillette, J., Caillierez, R., Zommer, N., Alves-Pires, C., Benilova, I., Blum, D., De Strooper, B., and Buée, L. (2012) Neurotoxicity and memory deficits induced by soluble low-molecular-weight amyloid-β1-42 oligomers are revealed in vivo by using a novel animal model. *J Neurosci* **32**, 7852-7861
37. Hille, B. (1978) Ionic Channels in Excitable membranes. *Biophysical Journal* **22**, 283--294
38. Hille, B. (1968) Pharmacological Modifications of the Sodium Channels of Frog Nerve. *The Journal of General Physiology* **51**, 199--219
39. Spangler, S. G. (1972) Expansion of the constant field equation to include both divalent and monovalent ions. *Alabama Journal of Medical Sciences* **9**, 218--223
40. Kawahara, M., Arispe, N., Kuroda, Y., and Rojas, E. (1997) Alzheimer's disease amyloid beta-protein forms Zn(2+)-sensitive, cation-selective channels across excised membrane patches from hypothalamic neurons. *Biophysical journal* **73**, 67--75

41. Näslund, J., Haroutunian, V., Mohs, R., Davis, K. L., Davies, P., Greengard, P., and Buxbaum, J. D. (2000) Correlation between elevated levels of amyloid beta-peptide in the brain and cognitive decline. *JAMA* **283**, 1571-1577
42. Prangkio, P., Yusko, E. C., Sept, D., Yang, J., and Mayer, M. (2012) Multivariate Analyses of Amyloid-Beta Oligomer Populations Indicate a Connection between Pore Formation and Cytotoxicity. *PLoS ONE* **7**
43. Narayan, P., Ganzinger, K. A., McColl, J., Weimann, L., Meehan, S., Qamar, S., Carver, J. A., Wilson, M. R., St George-Hyslop, P., Dobson, C. M., and Klenerman, D. (2013) Single molecule characterization of the interactions between amyloid-β peptides and the membranes of hippocampal cells. *J Am Chem Soc* **135**, 1491-1498
44. Qiu, L., Buie, C., Reay, A., Vaughn, M. W., and Cheng, K. H. (2011) Molecular dynamics simulations reveal the protective role of cholesterol in β-amyloid protein-induced membrane disruptions in neuronal membrane mimics. *J Phys Chem B* **115**, 9795-9812
45. Jang, H., Arce Fernando, T., Capone, R., Ramachandran, S., Lal, R., and Nussinov, R. (2009) Misfolded amyloid ion channels present mobile β-sheet subunits in contrast to conventional ion channels. *Biophysical Journal* **97**, 3029--3037
46. Lasagna-Reeves, C. A., Glabe, C. G., and Kayed, R. (2011) Amyloid-β annular protofibrils evade fibrillar fate in Alzheimer disease brain. *Journal of Biological Chemistry* **286**, 22122--22130
47. Mobley, D. L., Cox, D. L., Singh, R. R. P., Maddox, M. W., and Longo, M. L. (2004) Modeling amyloid beta-peptide insertion into lipid bilayers. *Biophysical journal* **86**, 3585--3597
48. Ashley, R. H., Harroun, T. A., Hauss, T., Breen, K. C., and Bradshaw, J. P. (2006) Autoinsertion of soluble oligomers of Alzheimer's Aβ(1–42) peptide into cholesterol-containing membranes is accompanied by relocation of the sterol towards the bilayer surface. *BMC Structural Biology* **6**
49. Meleleo, D., Galliani, A., and Notarachille, G. (2013) AβP1-42 incorporation and channel formation in planar lipid membranes: the role of cholesterol and its oxidation products. *J Bioenerg Biomembr* **45**, 369-381
50. Arispe, N. (2004) Architecture of the Alzheimer's A beta P ion channel pore. *The Journal of membrane biology* **197**, 33--48
51. Durell, S. R., Guy, H. R., Arispe, N., Rojas, E., and Pollard, H. B. (1994) Theoretical models of the ion channel structure of amyloid beta-protein. *Biophysical journal* **67**, 2137--2145
52. Peters, C., Sepúlveda, F. J., Fernández-Pérez, E. J., Peoples, R. W., and Aguayo, L. G. (2016) The Level of NMDA Receptor in the Membrane Modulates Amyloid-β Association and Perforation. *J Alzheimers Dis* **53**, 197-207
53. Hong, S., Ostaszewski, B. L., Yang, T., O'Malley, T. T., Jin, M., Yanagisawa, K., Li, S., Bartels, T., and Selkoe, D. J. (2014) Soluble Aβ oligomers are rapidly sequestered from brain ISF in vivo and bind GM1 ganglioside on cellular membranes. *Neuron* **82**, 308-319
54. Arispe, N., and Doh, M. (2002) Plasma membrane cholesterol controls the cytotoxicity of Alzheimer's disease AbetaP (1-40) and (1-42) peptides. *FASEB J* **16**, 1526-1536
55. Ding, H., Schauerte, J. A., Steel, D. G., and Gafni, A. (2012) β-Amyloid (1-40) peptide interactions with supported phospholipid membranes: a single-molecule study. *Biophys J* **103**, 1500-1509
56. Johansson, A. S., Berglind-Dehlin, F., Karlsson, G., Edwards, K., Gellerfors, P., and Lannfelt, L. (2006) Physiochemical characterization of the Alzheimer's disease-related peptides A beta 1-42Arctic and A beta 1-42wt. *FEBS J* **273**, 2618-2630
57. Younan, N. D., and Viles, J. H. (2015) A Comparison of Three Fluorophores for the Detection of Amyloid Fibers and Prefibrillar Oligomeric Assemblies. ThT (Thioflavin T); ANS (1-Anilinonaphthalene-8-sulfonic Acid); and bisANS (4,4'-Dianilino-1,1'-binaphthyl-5,5'-disulfonic Acid). *Biochemistry* **54**, 4297-4306
58. Rice, W. (1989) Analyzing tables of statistical tests. ***Evolution*** **43**, 223-225

59. Cruickshank, C. C., and Minchin, R. F. (1997) Estimation of the Pore Size of the Large-Conductance Mechanosensitive Ion Channel of Escherichia coli. *Biophysical journal* **73**, 1925--1931
60. Schlumberger. (2009) Log Interpretation Charts. *Schlumberger*, 310

FOOTNOTES

This work was supported by the Life Science initiative, Queen Mary, University of London and the Biotechnology and Biological Sciences Research Council (BBSRC) Code: BB/M023877/1.

The abbreviations used are: Aβ, amyloid-β; AD, Alzheimer's disease; AFM, atomic force microscopy; GHK, Goldman Hodgkin Katz; LTP, long-term potentiation; SEC, size-exclusion chromatography; TEM, transmission electron microscopy; ThT, thioflavin-T.

FIGURE LEGENDS

FIGURE 1. Structurally distinct Aβ(1-40) and Aβ(1-42) preparations have markedly different abilities to induce ion-channel currents. a: *Left:* Thioflavin T fibre growth kinetics were monitored for solubilised Aβ(1-40) (blue), solubilised Aβ(1-42) (orange) and SEC- purified Aβ(1-42) (red) at 10 μM Aβ concentration (4 wells per preparation). *Right:* Voltage-ramp protocol applied to clamp cell membrane at six membrane step-potentials. Current was recorded at each potential and two representative traces recorded from separate membrane patches are shown with corresponding TEM images for Aβ(1-40) b: oligomer c: fibre and Aβ(1-42) d: monomer e: oligomer and a single representative trace for both f: oligomer-containing fibre and purified fibre preparations. All Aβ preparations were 5 μM (monomer equivalent) at pH 7.4. *TEM scale bar = 50 nm*

FIGURE 2. Channel formation observed in oligomeric Aβ(1-42) preparations but not with Aβ(1-40)**.** Proportion of membrane patches which form channels formed for monomeric, oligomeric and fibrillar Aβ(1-40) and Aβ(1-42). Channel formation was significant for Aβ(1-42) oligomer and oligomer containing fibre samples while corresponding Aβ(1-40) preparations were unable to form ion-channels, within 30 mins. Removal of the majority of small, diffusible oligomers from Aβ(1-42) fibre preparations significantly reduces the probability of channel formation. Data has been collected from n = 20 for each Aβ(1-40) preparation, n = 24 for Aβ(1-42) monomer and oligomer-depleted fibre, and n = 49 for Aβ(1-42) oligomer. 20 experimental repeats were also performed for buffer control samples.

FIGURE 3. Endogenous HEK293 ion channels are markedly different to Aβ(1-42) ion channels. a: Current traces recorded from three different membrane patches containing endogenously-expressed ion-channels. Endogenous ion-channels are at least three times smaller in conductance (<85 pS) than Aβ(1-42) channels and display comparatively short open times, rarely remaining open for more than 300 ms. Voltage-dependence and channel rectification were also commonly observed features, with the majority only opening at depolarising potentials. b: Example of the smallest sub-type of Aβ(1-42) channel formed by

Aβ(1-42) oligomers which displays typically observed features such as large conductance, long open times and voltage-independence. Current traces were recorded using voltage-ramp protocol outlined in Figure 1.

FIGURE 4. Aβ(1-42) channels exhibit multiple-conductance behaviour typically associated with Aβ ion channels. Two distinct conductance behaviours are transiently observed: **a)** rapid flicker between low and high conductance states and **b)** step transitions between conductance levels. Measured conductance states are highlighted by dashed lines. Grey solid lines represent zero baseline current. Currents are recorded from membrane patches held at a +60 mV potential with a Aβ(1-42) ion-channel incorporated.

FIGURE 5. Aβ(1-42) oligomer forms discrete ion channels of varying pore diameter. **a:** Current traces recorded from separate Aβ(1-42) channels which represent three commonly observed channel sizes. **b:** Conductance was calculated by generating a current-voltage relationship for each channel. Each dataset is composed of 30 channel current measurements across six membrane potentials and fitted with a linear regression. **c:** Conductance distribution of channels formed in the presence of Aβ(1-42) oligomer, and oligomer-containing fibre samples. Primary y-axis represents a rank order of conductance with increasing magnitude for 34 channels. Three discrete channel subtypes are highlighted (within a 50 pS range) and labelled by a median calculated pore diameter. A secondary y-axis accounts for bar-chart representation of the proportion of channels formed within a 50 pS bin size

FIGURE 6. Time elapsed before channel formation plotted against the cumulative proportion of channels formed by Aβ(1-42) oligomer with 5 μM Aβ (monomer equivalent concentration). At 0 minutes, patch-clamp recording is commenced on excision of a patch, where Aβ is free to diffuse towards the membrane. A ≥ 2 minute lag time precedes Aβ insertion and channel formation, with the bulk of channels incorporating between 4 to 7 minutes. The time taken for 50% of channels to form is indicated by a dashed line, at 8.5 minutes.

FIGURE 7. Current-voltage relationships suggest Aβ(1-42) channels are non-selective and are able to permeate both anions and cations. Channel reversal potential (E_{rev}) was recorded by measurement of channel current over seven voltage steps. a: The E_{rev} of channels pre-formed in symmetrical buffer was measured to be 0 mV (black □, n = 4). Replacement of NaCl with TEACl by 50% (blue ○, n = 2) and ~75% (red ◊, n = 2) minimally shifts E_{rev} to 6 mV. b: A second solution in which 80% of anions and cations were also replaced with non-polar sucrose was also exposed to three other channels. E_{rev} shifted from 0 mV in symmetrical solution (black □, n = 3) to – 8 mV (yellow ○, n = 3). Error bars represent standard deviation.

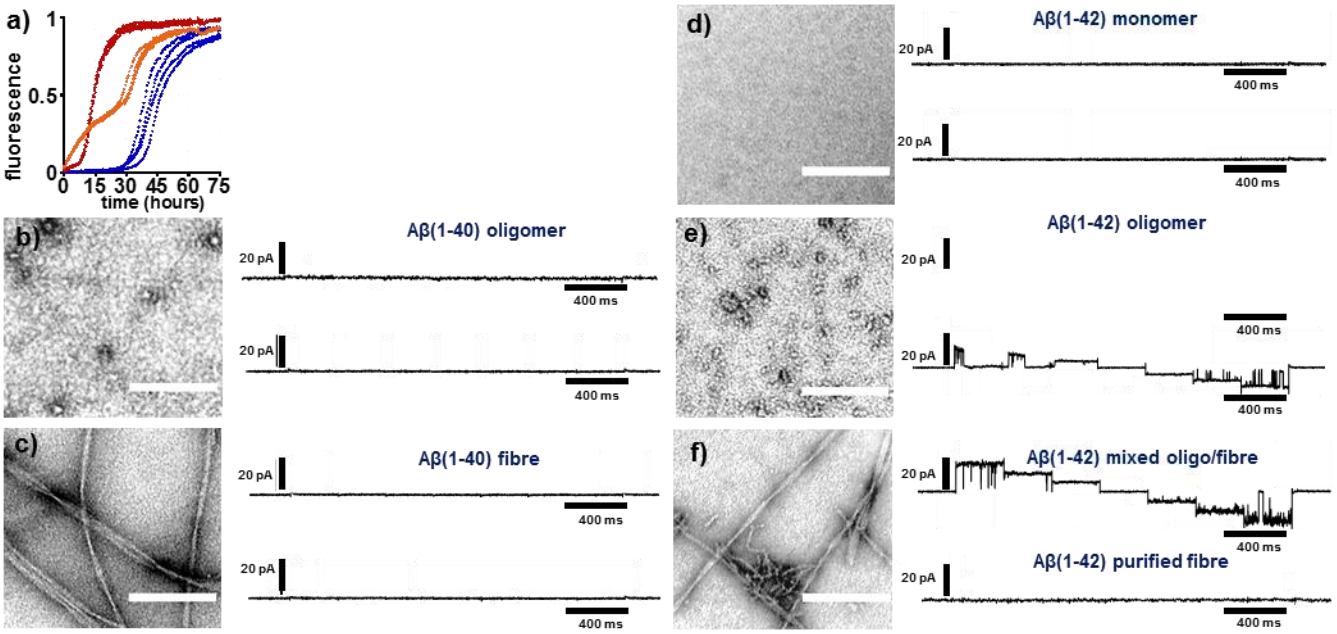

FIGURE 1. Structurally distinct Aβ(1-40) and Aβ(1-42) preparations have markedly different abilities to induce ion-channel currents. **a:** *Left:* Thioflavin T fibre growth kinetics were monitored for solubilised Aβ(1-40) (blue), solubilised Aβ(1-42) (orange) and SEC- purified Aβ(1-42) (red) at 10 μM Aβ concentration (4 wells per preparation). *Right:* Voltage-ramp protocol applied to clamp cell membrane at six membrane step-potentials. Current was recorded at each potential and two representative traces recorded from separate membrane patches are shown with corresponding TEM images for Aβ(1-40) **b:** oligomer **c:** fibre and Aβ(1-42) **d:** monomer **e:** oligomer and a single representative trace for both **f:** oligomer-containing fibre and purified fibre preparations**.** All Aβ preparations were 5 μM (monomer equivalent) at pH 7.4. *TEM scale bar = 50 nm.*

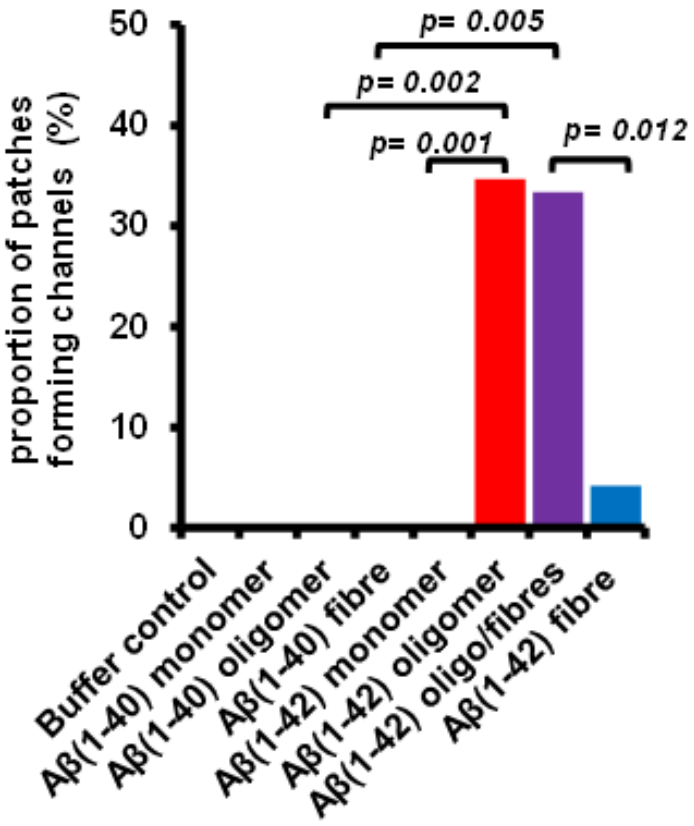

FIGURE 2. Channel formation observed in oligomeric Aβ(1-42) preparations but not with Aβ(1-40)**.** Proportion of membrane patches which form channels formed for monomeric, oligomeric and fibrillar Aβ(1-40) and Aβ(1-42). Channel formation was significant for Aβ(1-42) oligomer and oligomer containing fibre samples while corresponding Aβ(1-40) preparations were unable to form ion-channels, within 30 mins. Removal of the majority of small, diffusible oligomers from Aβ(1-42) fibre preparations significantly reduces the probability of channel formation. Data has been collected from n = 20 for each Aβ(1-40) preparation, n = 24 for Aβ(1-42) monomer and oligomer-depleted fibre, and n = 49 for Aβ(1-42) oligomer. 20 experimental repeats were also performed for buffer control samples.

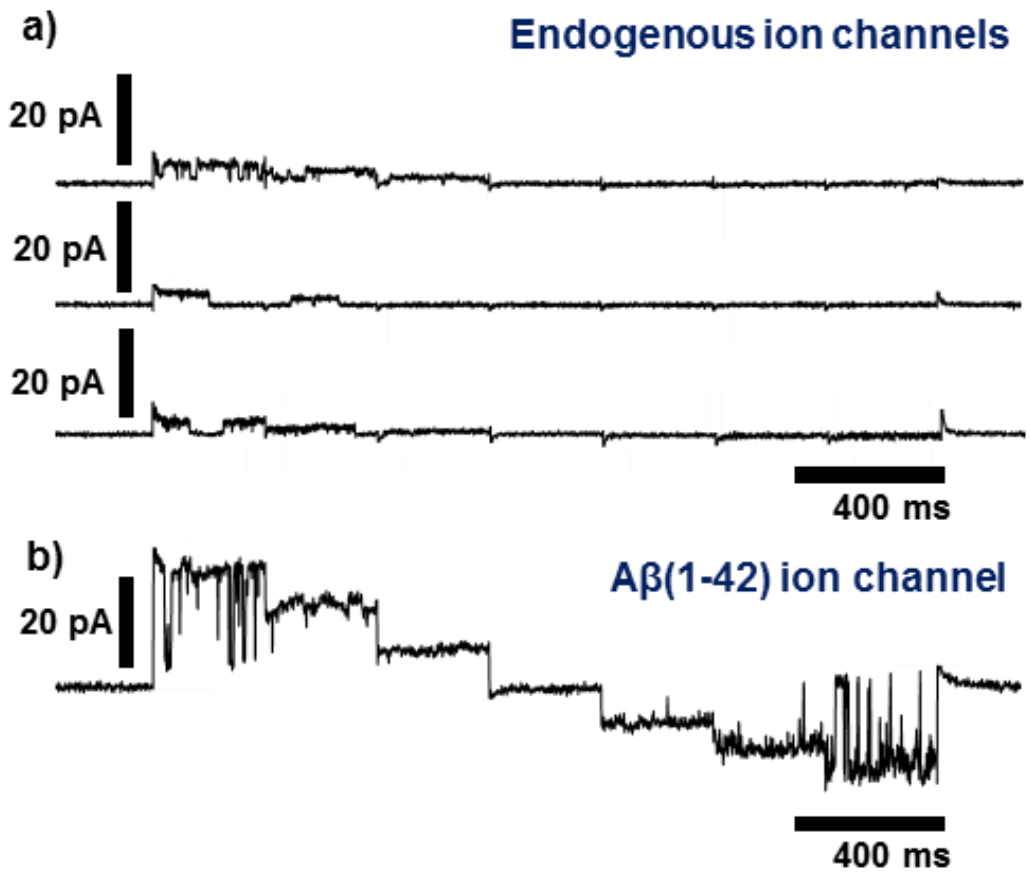

FIGURE 3. Endogenous HEK293 ion channels are markedly different to Aβ(1-42) ion channels. **a:** Current traces recorded from three different membrane patches containing endogenously-expressed ion-channels. Endogenous ion-channels are at least three times smaller in conductance (<85 pS) than Aβ(1-42) channels and display comparatively short open times, rarely remaining open for more than 300 ms. Voltage-dependence and channel rectification were also commonly observed features, with the majority only opening at depolarising potentials. **b:** Example of the smallest sub-type of Aβ(1-42) channel formed by Aβ(1-42) oligomers which displays typically observed features such as large conductance, long open times and voltage-independence. Current traces were recorded using voltage-ramp protocol outlined in Figure 1.

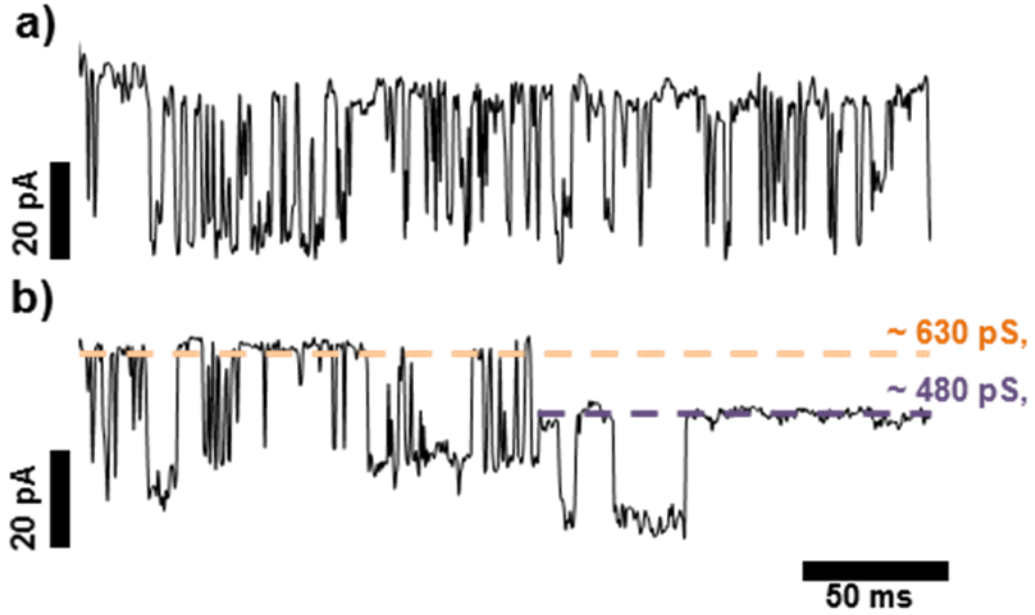

FIGURE 4. Aβ(1-42) channels exhibit multiple-conductance behaviour typically associated with Aβ ion channels. Two distinct conductance behaviours are observed: **a)** rapid flicker between low and high conductance states and **b)** step transitions between conductance levels. Measured conductance states are highlighted by dashed lines and approximate pore diameter is estimated. Grey solid lines represent zero baseline current. Currents are recorded from membrane patches held at a +60 mV potential with a Aβ(1-42) ion-channel incorporated.

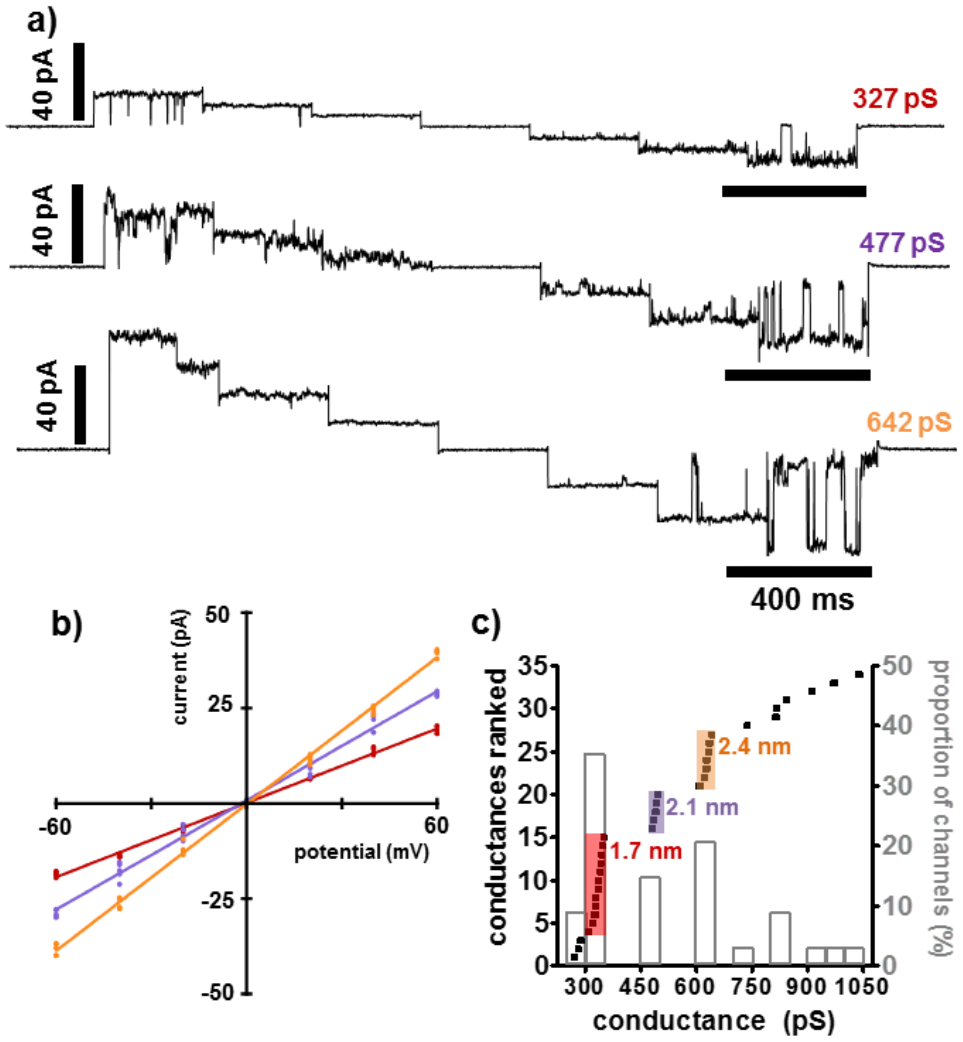

FIGURE 5. Aβ(1-42) oligomer forms discrete ion channels of varying pore diameter. **a:** Current traces recorded from separate Aβ(1-42) channels which represent three commonly observed channel sizes. **b:** Conductance was calculated by generating a current-voltage relationship for each channel. Each dataset is composed of 30 channel current measurements across six membrane potentials and fitted with a linear regression. **c:** Conductance distribution of channels formed in the presence of Aβ(1-42) oligomer, and oligomer-containing fibre samples. Primary y-axis represents a rank order of conductance with increasing magnitude for 34 channels. Three discrete channel subtypes are highlighted (within a 50 pS range) and labelled by a median calculated pore diameter. A secondary y-axis accounts for bar-chart representation of the proportion of channels formed within a 50 pS bin size.

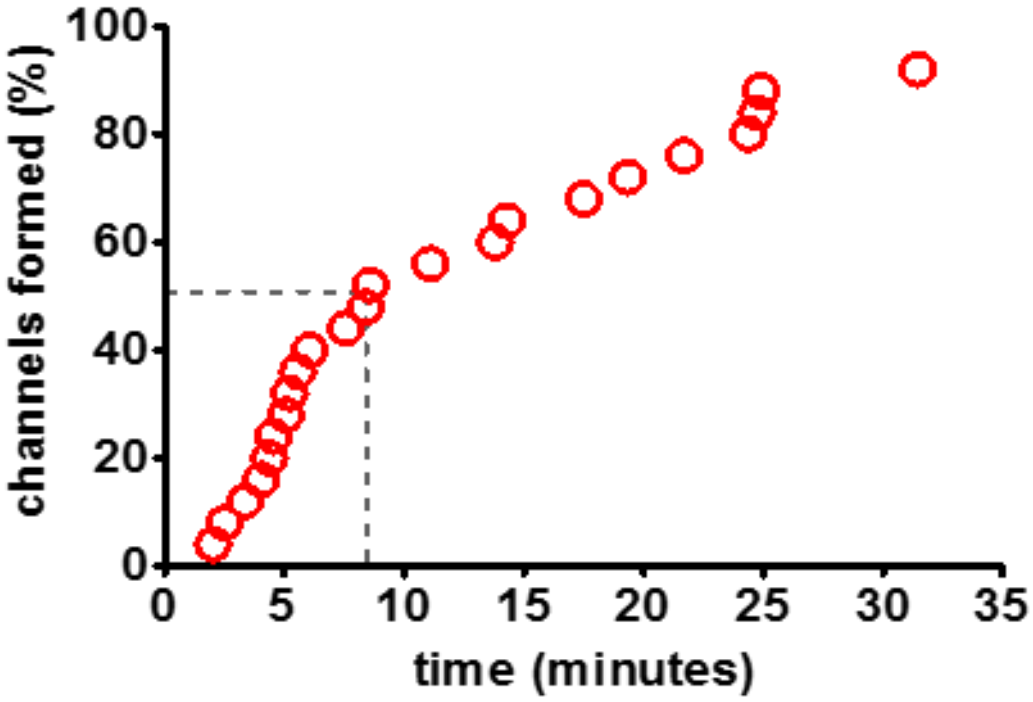

FIGURE 6. Time elapsed before channel formation plotted against the cumulative proportion of channels formed by Aβ(1-42) oligomer with 5 μM Aβ (monomer equivalent concentration). At 0 minutes, patch-clamp recording is commenced on excision of a patch, where Aβ is free to diffuse towards the membrane. A ≥ 2 minute lag time precedes Aβ insertion and channel formation, with the bulk of channels incorporating between 4 to 7 minutes. The time taken for 50% of channels to form is indicated by a dashed line, at 8.5 minutes.

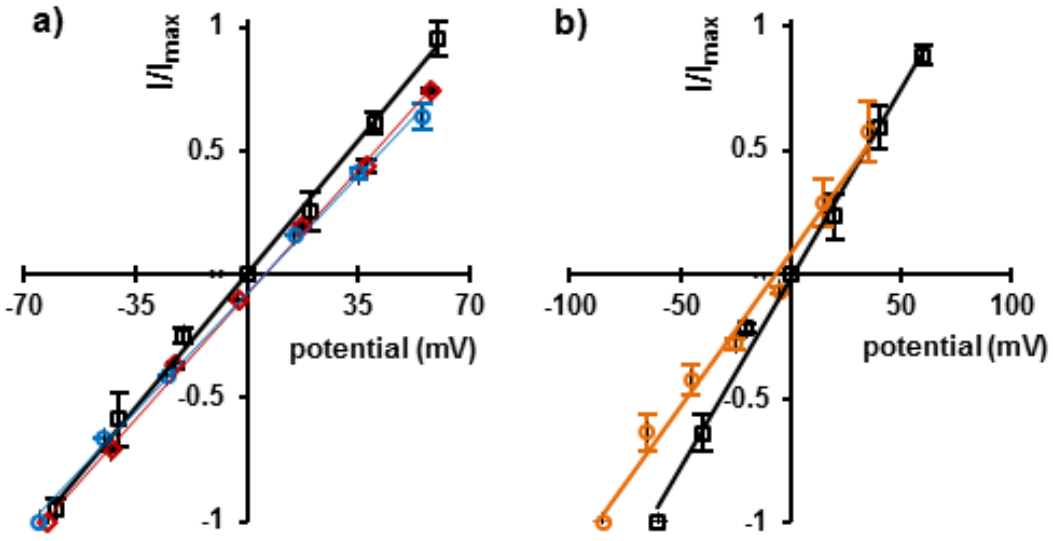

FIGURE 7. Current-voltage relationships suggest Aβ(1-42) channels are non-selective are are able to permeate both anions and cations. Channel reversal potential (E_{rev}) was recorded by measurement of channel current over seven voltage steps. **a:** The E_{rev} of channels pre-formed in symmetrical buffer was measured to be 0 mV (black □, n = 4). Replacement of NaCl with TEACl by 50% (blue ○, n = 2) and ~75% (red ◊, n = 2) minimally shifts Erev to 6 mV. **b:** A second solution in which 80% of anions and cations were also replaced with non-polar sucrose was also exposed to three other channels. E_{rev} shifted from 0 mV in symmetrical solution (black □, n = 3) to – 8 mV (yellow ○, n = 3). Error bars represent standard deviation.